Modification of Cellulose Nanocrystals with Quaternary Ammonium-Containing Hyperbranched Polyethylene Ionomers by Ionic Assembly

Lingqi Huang,[1] Zhibin Ye,[1,*] and Richard Berry[2]

1. School of Engineering, Laurentian University, Sudbury, Ontario P3E 2C6, Canada

2. CelluForce Inc, Montreal, Quebec H3A 1K2, Canada

* Corresponding author; email: zye@laurentian.ca

Abstract

We demonstrate in this article the first surface modification of cellulose nanocrystals (CNCs) with quaternary ammonium-containing ionomers by ionic binding of their positively charged ammonium ions onto the negatively charged surface of CNCs. A range of hyperbranched polyethylene ionomers (I1–I6) having different ionic content (0.2–2.3 mol%) has been designed and employed for this purpose. The simple dropwise addition and mixing of the aqueous dispersion of CNCs with the ionomer solution in tetrahydrofuran (THF) conveniently renders the ionomer-modified CNCs (mCNC1–mCNC6). The presence of adsorbed ionomers on the modified CNCs is confirmed with spectroscopic and x-ray diffraction evidence, and quantified through thermogravimetric analysis. The effects of the ionomer to CNC feed mass ratio and the ionomers of different ionic content on the modification have been examined. A study on the morphology of the modified CNCs by atomic force microscopy discloses the occurrence of side-to-side and/or end-to-end assembly of the CNC rods due to the "cross-linking" or bridging effects of the multidentate ionomers. Because of the hydrophobic hyperbranched polyethylene segments in the adsorbed ionomers, the modified CNCs can be dispersed in nonpolar or low-polarity organic solvents (such as THF, toluene, and chloroform). In particular, the THF dispersions of modified CNCs prepared with ionomers having ionic content ≥ 0.7 mol% (I3–I6) behave as thixotropic organo-gels at concentrations ≥ 40 mg mL^{-1}. Further, the modified CNCs better disperse than unmodified CNCs in a hydrophobic ethylene-olefin copolymer (EOC) elastomer matrix and

show better thermal stability than a surfactant-modified CNC sample. Tensile testing confirms that the EOC composites, filled with the ionomer-modified CNCs, are significantly reinforced with a tensile modulus nearly doubled that of neat EOC, and better elongation at break relative to those filled with unmodified CNCs or surfactant-modified CNCs.

Keywords: cellulose nanocrystals, modification, ionomers, composites, dispersion, reinforcement, bionanofiller

■ Introduction

Cellulose nanocrystals (CNCs) extracted from abundant and renewable biosources have been receiving extensive attention.[1-6] Having a rod-like shape with generally a diameter between 5 and 15 nm and a length between 100 and 300 nm, CNCs have high elastic moduli (over 100 GPa), high specific surface area (several hundred m^2/g), and a reactive surface while being low density.[7] As such, they have been widely investigated, since the first demonstration in 1995,[8] as the reinforcing bionanofillers for the construction of polymer nanocomposites with significantly enhanced mechanical properties.[9-11]

CNCs are generally produced as stable aqueous dispersions often by sulfuric acid hydrolysis of cellulose fibers. Their surface is highly polar and negatively charged due to the presence of sulfate groups resulting from sulfuric acid hydrolysis.[1-6] Most applications of CNCs have thus focused on the aqueous systems by mixing aqueous CNC dispersions with various compatible water-soluble or water-dispersible components (such as water-soluble monomers and polymers,[12-21] water-dispersible nanoparticles[22-24] and latexes,[25-29] etc.) to obtain functional composite materials. In particular, water-soluble hydrophilic polymers or water-dispersible latexes, including poly(vinyl alcohol),[17,18] poly(ethylene oxide),[19,20] poly(furfuryl alcohol),[21] latexes of poly(styrene-co-butyl acrylate), poly(styrene-co-butadiene), and polybutadiene,[26-29] etc., have been employed as the compatible polymer matrices for the construction of CNC-reinforced polymer nanocomposites by solution mixing. CNCs can be well dispersed in these polar polymer matrices, which maximizes the reinforcement. However, without proper

surface modification, the dispersion of CNCs in nonpolar solvents or hydrophobic polymers, such as polyolefins which are produced in the largest volume, are poor.[1-5,9-11,30,31]

To broaden their application scope, surface modification of CNCs through both covalent and noncovalent approaches has been attempted to modify their surface properties so as to render their dispersibility in organic solvents (particularly, nonpolar and low-polarity solvents) and hydrophobic polymer matrices.[1-5,9-11,30,31] In the covalent approaches, desired organic groups are directly attached onto the surface of CNCs through the hydroxyl groups present on their surface. Various polymers have also been covalently grafted onto the surface of CNCs through both graft-from[32-34] and graft-to strategies.[35-37] Though highly effective, these covalent surface modification methods often involve tedious and delicate reaction/polymerization chemistry and are inconvenient. In the noncovalent approaches, CNCs are often modified with surfactants through their adsorption via noncovalent electrostatic attraction, hydrophilic affinity, hydrogen bonding, or van der Waals interactions.[30,31] Thus far, various surfactants (anionic, cationic, and nonionic),[32,38-44] as well as specifically designed block polymers,[25,45] have been employed, rendering the modified CNCs with good dispersibility in desired nonpolar organic solvent or polymer matrices. Relative to covalent ones, these noncovalent approaches are more convenient and easier to implement. However, the amount of surfactant required to cover CNCs is often high, along with the highly possible desorption of the adsorbed surfactant given the involvement of only weak monodentate noncovalent interactions, which could undermine the properties of the resulting composites.[11,40]

In this paper, we demonstrate the convenient noncovalent surface modification of CNCs with the use of a new range of quaternary ammonium-containing hyperbranched polyethylene ionomers. Ionomers are polymers containing a small fraction of ionic functional groups (typically less than 10 mol%) that are covalently bonded to the polymer backbone as pendant groups. Designed with positively charged quaternary ammonium ions tethered onto the nonpolar hyperbranched polyethylene skeleton, these ionomers have been found to bind to the negatively charged surface of CNCs through multidentate ionic interactions, rendering

modified CNCs as self-assembled CNC/ionomer composites. The modified CNCs have been thoroughly characterized with various techniques for their compositional, structural, thermal, and morphological features. They have also been investigated for their dispersion in various nonpolar or low-polarity organic solvents and a commercial hydrophobic ethylene-octene copolymer (EOC) matrix. The dispersions have been systematically characterized, with the enhanced dispersibility of the modified CNCs in these media and improved properties demonstrated. Though various quaternary ammonium-containing surfactants[42-44] or polyelectrolytes[25,46,47] have been previously employed for the modification of CNCs, this is the first report on the use of quaternary ammonium-containing ionomers with a hydrophobic skeleton for rendering modified CNCs.

■ Experimental Section

Materials

An aqueous dispersion of CNCs (concentration: 21 mg/mL; the length and average diameter of 150 and ~5 nm) prepared by sulfuric acid hydrolysis of bleached softwood kraft was obtained from CelluForce (Canada) and was subjected to purification by dialysis with deionized water. The Pd–diimine catalyst, [(ArN=C(Me)−(Me)C=NAr)Pd(CH_3)(N≡CMe)]$^+SbF_6^-$ (Ar = 2,6-(iPr)$_2C_6H_3$), was synthesized according to the literature procedure.[48] The acrylate-type ionic liquid comonomer, [2-(acryloyloxy)ethyl] trimethylammonium tetrafluoroborate ($AETMA^+BF_4^-$) was prepared from [2-(acryloyloxy)ethyl]trimethylammonium chloride (80 wt% aqueous solution, Aldrich) via anion exchange with $NaBF_4$ (Aldrich) by following a procedure reported in our earlier paper.[49] Ethylene (polymer grade) was obtained from Praxair Canada and was purified by passing through purification columns. Acetone (certified ACS grade, Fisher Scientific) was dehydrated with molecular sieves before use. The EOC used herein as the polymer matrix for the compounding of polymer nanocomposites is Engage 8130 obtained from Dow Chemical, which is an ethylene-octene copolymer with the octene comonomer content of 42 wt%. It has

a density of 0.864 g cm^{-3}, a melt flow index of 13 g min^{-1} (at 190 ºC). Cetyltrimethylammonium bromide (CTAB, ≥ 98%) was obtained from Sigma. All other reagents or solvents were obtained from either Aldrich or Fisher Scientific and were used as received.

Synthesis of Hyperbranched Polyethylene Ionomers

The hyperbranched polyethylene ionomers (I1–I6) were synthesized by direct copolymerization of ethylene with ionic liquid comonomer $AETMA^+BF_4^-$ by following the procedure reported in our earlier paper.[49] The polymerization reactions were all carried out in a 50 mL Schlenk flask equipped with a magnetic stirrer. The flask sealed with a rubber septum was first flame-dried under vacuum. After being cooled down to room temperature, the reactor was purged with ethylene for at least three times, and then filled with ethylene to 1 atm (absolute pressure). A solution of the ionic liquid comonomer (0.245–2.45 g in 5 mL of dry acetone) was then injected into the reactor. Subsequently, the polymerization was started upon the injection of the Pd–diimine catalyst solution (0.08 g, 0.1 mmol in 5 mL of dry acetone). During the polymerization, ethylene pressure was maintained constant by continuous feed from a cylinder and the polymerization temperature was maintained at room temperature with a water bath. After 24 h, the polymerization was stopped by shutting down the ethylene supply and venting the reactor. The black product containing Pd(0) particles resulting from the decomposition of the Pd–diimine catalyst was precipitated out with a large amount of methanol. The precipitate was redissolved in a small amount of THF for multiple washings with methanol. The polymer precipitate was purified to remove Pd black (see our earlier paper[49]) and then dried under vacuum at room temperature, rendering ionomers. As per ^1H NMR spectroscopy, the resulting ionomers (I1–I6) contain quaternary ammonium ion content of 0.2, 0.4, 0.7, 1.1, 1.5, and 2.3 mol%, respectively.

Preparation of Ionomer-Modified CNCs

Typically, the hyperbranched polyethylene ionomer (5–40 mg) was dissolved in THF (40 mL).

Under ultrasonication, the aqueous CNC dispersion (10 mg in 0.5 mL) was added dropwise into the ionomer solution. The resulting dispersion was further ultrasonicated for ca. 15 min and was then vacuum-filtered on a PTFE membrane (0.22 μm pore size). The filter cake was thoroughly washed with fresh THF, then dried under vacuum at ca. 50 ºC to render the modified CNCs.

Preparation of CTAB-Modified CNCs

CTAB-modified CNCs were prepared by following a literature procedure[44] with minor modifications. The original CNC aqueous dispersion was diluted to a concentration of 5 mg mL^{-1}, with the adjustment of its pH to 10 by the addition of a NaOH solution. Subsequently, the CNC dispersion (120 mL) was added dropwise into an aqueous CTAB solution (120 mL at 5 mg mL^{-1}) at 60 ºC under vigorous stirring. The mixture was continuously stirred at 60 ºC for 3 h, and then stirred overnight at room temperature. Afterwards, unbound CTAB was removed by dialysis with about 20 water changes. Freeze-drying of the resulting dispersion rendered the CTAB-modified CNCs (610 mg), termed as CTAB-CNC. The CTAB content in CTAB-CNC was 15 wt% (as per thermogravimetric analysis).

Preparation of EOC Composites

The EOC composites were prepared by a solution compounding method. A prescribed quantity of modified CNCs (equivalent to 10 wt% of neat CNCs in composites) was dispersed at 10 mg mL^{-1} in toluene by ultrasonication for 24 h. In the case with original unmodified CNCs, freeze-dried CNCs were dispersed in THF at 10 mg mL^{-1}. The dispersion was added dropwise into a toluene solution of EOC (50 mg mL^{-1}) within 1 h under magnetic stirring. The mixture was continuously stirred for 3 h before precipitation in a large amount of methanol. The precipitate was dried at 120 ºC in a vacuum oven for 24 h.

Characterizations and Measurements

^{1}H NMR spectra of the ionomers were all collected on a Varian Gemini 2000 spectrometer (200 MHz) with $CDCl_3$ as the solvent. Average molecular weights and dilute solution properties of the ionomers were measured with a triple-detection gel permeation chromatography (GPC) equipped with a three-angle light scattering detector, a refractive index concentration detector, and a viscosity detector in THF at 33 ºC. Please refer to our earlier paper.[49] Fourier-transformed infrared (FTIR) spectra were obtained on a Thermo Scientific Nicolet 6700 Analytical FTIR spectrometer. The samples were prepared as pellets using spectroscopic-grade KBr. Thermogravimetric analysis (TGA) was carried out on a TA Instruments Q50 thermogravimetric analyzer. Measurements were performed in a N_2 atmosphere with a continuous flow of 60 mL min^{-1} through the sample furnace and a flow of 40 mL min^{-1} through the balance compartment. In a typical measurement, the sample (ca. 5 to 10 mg) was heated from 30 to 800 ºC at 10 ºC min^{-1}. Differential scanning calorimetry (DSC) measurements were performed on a TA Instruments Q100 DSC equipped with a refrigerated cooling system (RCS) under a N_2 atmosphere at a flow of 50 mL min^{-1}. The instrument was operated in the standard DSC mode and was calibrated with an indium standard. Samples (ca. 8 mg) were heated from 40 to 170 ºC at 10 ºC min^{-1}, held at 170 ºC for 3 min, and cooled to –90 ºC at 10 ºC min^{-1}, followed with a subsequent heating ramp from –90 to 170 ºC at 10 ºC min^{-1}.

Dynamic light scattering (DLS) measurements of the dilute dispersions (ca. 0.1 mg mL^{-1}) of the various CNC samples for their hydrodynamic particle size and ζ potential were performed on a Brookhaven NanoBrook Omni Instrument at 25 ºC. Wide-angle x-ray diffraction patterns of the ionomer and CNC samples were recorded on an X'Pert Pro diffractometer with Cu Kα radiation (wavelength 1.54 Å) at room temperature. Atomic force microscopy (AFM) imaging of the various CNC samples was performed on a Bruker multimode atomic force microscope in the tapping mode with a phosphorous-doped silicon tip having a force constant of 20–80 N m^{-1}. AFM samples were prepared by placing a freshly cleaved mica piece in the dilute dispersion (ca. 0.1 mg mL^{-1}) of the corresponding CNC sample overnight for sample deposition, which was then taken out and dried for the imaging.

Rheological characterizations of the organo-gels of modified CNCs in THF were performed on a TA Instruments AR-G2 rheometer through both small amplitude dynamic oscillation and steady shear measurements with a cone-plate geometry (2º in cone angle and 40 mm in diameter). To avoid evaporation of THF, the measurements were all undertaken at 10 ºC, which was maintained with a Pelletier plate temperature controlling system, along with the use of a solvent trap to minimize THF evaporation. For the dynamic oscillation measurements, the following procedure was used. A pre-shear at 50 s^{-1} was first performed to destroy the gel network structure. Then a dynamic oscillation frequency scan from 0.01 to 100 Hz was undertaken at a high strain of 100%. After resting for 15 min for the rebuilding of the gel network, the second dynamic oscillation frequency scan from 0.01 to 100 Hz was performed at a low strain of 0.01%. The steady shear measurements were done by increasing the shear rate from 0.0001 to 200 s^{-1}, followed with the decrease of shear rate from 200 to 0.0001 s^{-1}. Prior to each steady shear measurement, the sample was equilibrated for 15 min for the formation of the gel network.

Rheological characterizations of EOC and its various composites were performed on the same instrument with a 20 mm parallel plate geometry at a gap of 1 mm. The measurements were all carried out in the small amplitude dynamic oscillation mode at the strain of 0.1% within a frequency range of 0.01−100 Hz at 190 ºC. The temperature was maintained within ± 0.1 ºC with the electrically heated plate system and the measurements were done under N_2 protection. Rheology sample discs were prepared by compression molding in a Carver press at approximately 135 ºC for 1 min.

Tensile properties of nanocomposites were examined using an Instron 5943 universal tester equipped with a 1 KN load cell. All experiments were carried out with a crosshead speed of 500 mm min^{-1}. Type VI (ASTM D638) dog-bone shaped samples were cut from a sheet with an average thickness of 2.7 mm with a die. The sheets were prepared by compression molding in a Carver press at approximately 135 ºC for 1 min. Three repeat trials were performed for most specimens with two repeats for composites made in lower quantity and the average is reported.

■ Results and Discussion

Synthesis of Hyperbranched Polyethylene Ionomers

The hyperbranched polyethylene ionomers (I1–I6) containing the tetralkylammonium ions at different content were synthesized herein by Pd–diimine-catalyzed direct copolymerization of ethylene with $AETMA^+BF_4^-$ as the ionic liquid comonomer (see Scheme 1). Our group recently discovered this direct copolymerization strategy for convenient synthesis of quaternary ammonium-containing polyethylene ionomers and elucidated the structures and physical properties of these ionomers.[49] Table S1 in the Supporting Information summarizes the copolymerization conditions and detailed characterization results (including composition, branching structure, molecular weight, and dilute solution properties) of the ionomers. Figure S1 in the Supporting Information shows their ^1H NMR spectra, which confirm their possession of the covalently tethered quaternary ammonium ions and the highly branched polyethylene skeleton. Changing the feed concentration of $AETMA^+BF_4^-$ in the polymerization allows the convenient tuning of its content (*i.e.*, quaternary ammonium content; 0.2， 0.4， 0.7， 1.1， 1.5， and 2.3 mol% for I1–I6, respectively; see Table S1) in the ionomers.[49] In consequence, the average molecular weight (see Table S1) of the ionomers generally decreases with the increase of the quaternary ammonium content.[49] The quaternary ammonium ions are randomly distributed in the ionomer chains given the statistical Pd–diimine-catalyzed ethylene-acrylate copolymerization mechanism,[50,51] with each ionomer chain containing multiple ions on average. As per their low intrinsic viscosity (see Table S1), the polyethylene skeleton of these ionomers features a spherical dendrimer-like, highly compact hyperbranched chain architecture, resulting from the well-known chain walking mechanism of the Pd–diimine catalyst.[50,51] This hyperbranched architecture is beneficial since it completely disrupts the formation of polyethylene crystals and thus renders the ionomers with good dispersibility/solubility in nonpolar/low-polarity solvents (such as THF, toluene, chloroform, etc.), which facilitates the subsequent surface modification of CNCs through solution mixing. In the solvents, the ionomers form

3-dimensional physical cross-linking networks due to the aggregation of the quaternary ammonium ions.[49] DLS characterization of I4 as a representative ionomer in THF shows a large z-average hydrodynamic size of *ca*. 280 nm with a very broad size distribution (ranging from ca. 10 nm to 10,000 nm with polydispersity index, PDI = 0.56) and a ζ potential of *ca*. 10 mV. The large size and broad distribution provide the evidence supporting the presence ionic aggregation.

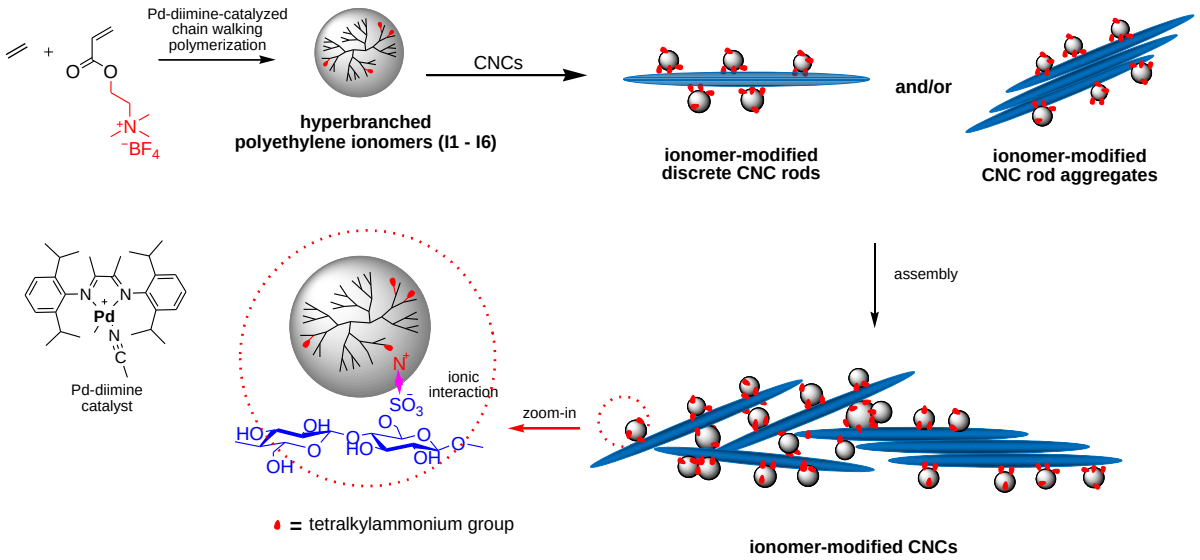

Scheme 1. Synthesis of hyperbranched polyethylene ionomers and their schematic modification of CNCs to form modified CNCs.

Surface Modification of CNCs with Various Ionomers

Aqueous dispersions of CNCs prepared by sulfuric acid hydrolysis of bleached softwood kraft fibers are employed in this study. Due to the presence of the surface sulfate groups resulting from sulfuric acid hydrolysis,[1-5,30,31] their surface is negatively charged with the ζ potential measured to be –27 mV. The quaternary ammonium-containing ionomers synthesized herein can thus bind onto the negatively charged CNCs through the multidentate ionic assembly when mixed, rendering surface-modified CNCs (see Scheme 1). We reason that the hydrophobic hyperbranched polyethylene segments in the adsorbed ionomers should facilitate the dispersion of the modified CNCs in both nonpolar/low polarity organic solvents

and hydrophobic polymer matrices, particularly polyethylene-derived polymer matrices (such as EOC herein), due to their structural compatibility. This will allow the subsequent convenient solution compounding of reinforced EOC composites with the use of modified CNCs as the reinforcing fillers.

Herein, surface modification of CNCs with the ionomers is conveniently achieved by the simple dropwise addition of an aqueous CNC dispersion (21 mg mL^{-1}) into a dilute solution of each ionomer in THF at desired concentrations under ultrasonication. In this procedure, the volume ratio of the aqueous CNC dispersion to the THF ionomer solution was made low, 1:80, to prevent the undesired precipitation of the ionomers upon the addition of excess water. During the dropwise addition of the CNC solution, the mixture became cloudy initially, followed with the gradual formation of fluffy white precipitates. The phenomenon is drastically different from the control experiment by dropping CNC solution into pure THF without containing ionomers, where visible large aggregates immediately formed. This difference clearly indicates the effect of the ionomers. The resulting mixture was vacuum-filtered; the solids were thoroughly washed with excess fresh THF to remove unused ionomers and then dried, rendering the modified CNCs as white solid powders. Through this procedure, we found that a nearly quantitative retention of the feed CNCs was achieved in all cases. In the case with I3 as the modifying ionomer, we investigated the effect of the feed mass ratio of ionomer to CNC [$(m_{ionomer}/m_{CNC})_0$, in the broad range of 0.5 to 4] on the modification by changing the concentration of the ionomer solution while with a fixed weight of CNCs. With the other ionomers, the $(m_{ionomer}/m_{CNC})_0$ ratio was set at 2 to investigate the effect of ionic content of the ionomer on the modification. The resulting modified ionomers are termed as mCNC# (*i.e.*, mCNC1 to mCNC6) with the number denoting the corresponding ionomers (I1, I2, I4 to I6), or mCNC3-# (*i.e.*, mCNC3-1 to mCNC3-4) for those modified with I3 at different $(m_{ionomer}/m_{CNC})_0$ ratios. Table 1 summarizes the characterization of these modified CNCs.

Figure 1 shows the FTIR spectrum of a representative modified CNC sample, mCNC4, as well as the spectra of the corresponding ionomer (I4) and dried original unmodified CNCs for

comparison. I4 shows two characteristic bands at 1737 and 1460 cm^{-1}, respectively. They correspond respectively to the C=O stretching frequency of the carbonyl group and the trimethyl groups of the quaternary ammonium in the incorporated $AETMA^{+}BF_4^{-}$ units in the ionomer.[42] These two bands are absent in the unmodified CNCs but are clearly present in mCNC4, thus confirming qualitatively the presence of the adsorbed ionomer in the modified CNC sample.

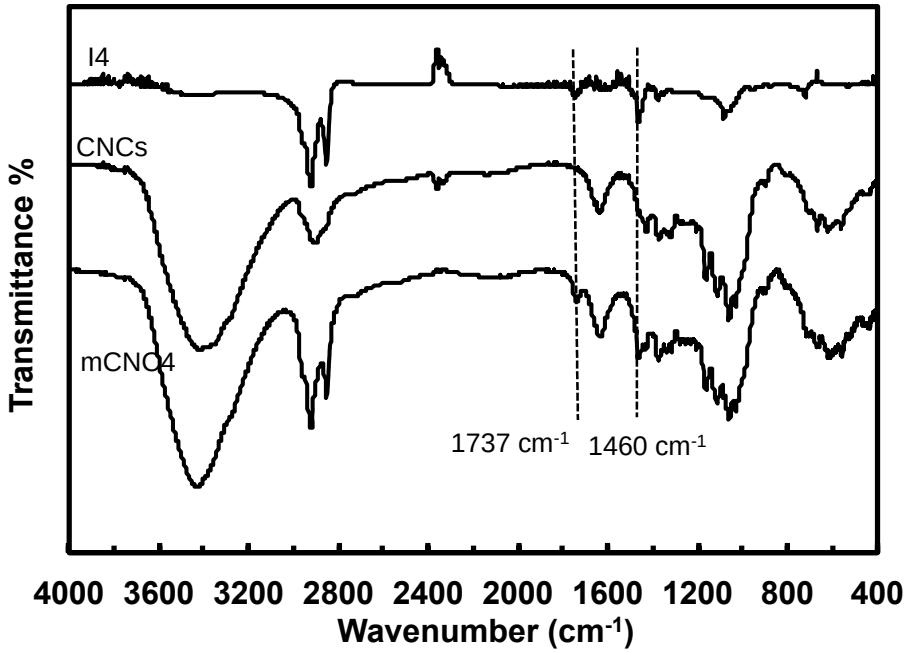

Figure 1. FTIR spectra of I4, dried original unmodified CNCs, and I4-modified mCNC4.

Table 1. Characterization of the modified CNCs prepared with different ionomers.

Modified CNCs	Ionomer	$(m_{ionomer}/m_{CNC})_0$[a]	TGA results				DLS results[e]		
			ΔW_1[b] (%)	ΔW_2[b] (%)	$T_{d,max}$[c] (°C)	Ionomer content[d] (wt%)	d_p (nm)	PDI	ζ potential (mV)
CNCs	N/A	0	63	16	311	0	91	0.3	-27
mCNC1	I1	2	58	32	311	8			
mCNC2	I2	2	51	38	311	19	401	0.39	-15
mCNC3-1	I3	0.5	58	34	314	8			
mCNC3-2	I3	1	52	41	314	17	273	0.37	17
mCNC3-3	I3	2	46	47	321	27	332	0.41	17
mCNC3-4	I3	4	41	50	323	35	255	0.39	22
mCNC4	I4	2	43	46	326	32	265	0.36	20
mCNC5	I5	2	46	44	320	27	552	0.56	22
mCNC6	I6	2	45	42	320	29	287	0.34	30

[a] Feed mass ratio of ionomer to CNC employed in the preparation of modified CNCs. [b] ΔW_1: percentage weight loss within the temperature range of 220–330 °C; ΔW_2: percentage weight loss within the temperature range of 330–500 °C. [c] Peak CNC-decomposition temperature. [d] Percentage ionomer mass content in the modified CNCs calculated according to: $Percentage\ of\ ionomer = 100 - \Delta W_1/0.63$. [e] Z-average hydrodynamic particle size (d_p), polydispersity index (PDI) for size distribution, and ζ potential determined by DLS from dilute dispersions in water (for original unmodified CNCs) or THF (for ionomer-modified CNCs).

TGA characterization was performed on the modified CNCs to evaluate their thermal behavior and quantify their ionomer content. Figure 2a shows the TGA curves of the I3-modified CNCs obtained at various $(m_{ionomer}/m_{CNC})_0$ ratios, along with those of I3 and dried unmodified CNCs for comparison. I3 starts decomposition at around 350 ºC with the nearly complete weight loss at 500 ºC (char yield of 0.5% at 500 ºC). Nearly identical TGA curves were observed with the other ionomers. Dried unmodified CNCs start decomposition at about 220 ºC and exhibit a drastic 63% weight loss within 220–330 ºC followed with a gradual weight loss upon the further temperature increase (with an additional weight loss of 16% within 320–500 ºC), which is typical of sulfonated CNCs.[52,53] All the I3-modified CNCs exhibit a well-separated two-step weight loss, with the first step within 220–330 ºC (ΔW_1) attributable solely to the decomposition of CNCs and the second step within 330–500 ºC (ΔW_2) resulting from the degradation of both CNCs and the ionomer. The mass content of the ionomer in the modified CNCs has thus been quantified from ΔW_1 and are summarized in Table 1. Figure 2b plots the dependence of the mass content of I3 in the I3-modified CNCs on the $(m_{ionomer}/m_{CNC})_0$ ratio. Increasing the $(m_{ionomer}/m_{CNC})_0$ ratio from 0.5 to 4 leads to a significant increase in the mass content of I3 from 8 to 35 wt%. This indicates the amount of adsorbed ionomer increases with its feed concentration. However, the increase in the ionomer mass content is much more significant within the $(m_{ionomer}/m_{CNC})_0$ ratio of 0.5–2. As such, the modification with the other ionomers was all undertaken at the $(m_{ionomer}/m_{CNC})_0$ ratio of 2.

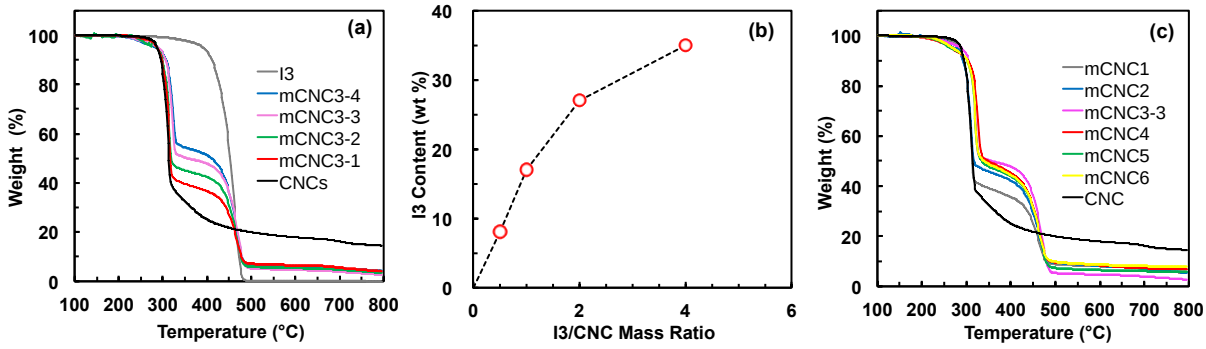

Figure 2. (a) TGA curves of I3, dried unmodified CNCs, and CNCs modified with I3 (mCNC3-1 to mCNC3-4) at different ionomer/CNC mass ratios; (b) effect of I3/CNC mass ratio on the content of I3 in the mCNC3 set of modified CNCs; (c) TGA curves of various modified CNCs prepared at the mass ratio of 2, along with that of unmodified CNCs for comparison.

Similar two-step TGA curves (see Figure 2c) were found with modified CNCs prepared with the other ionomers at the same $(m_{ionomer}/m_{CNC})_0$ ratio of 2. Except mCNC1 and mCNC2 having lower ionomer content of 8 and 19 wt%, respectively, the other modified CNCs all have similar ionomer content within 27–32 wt%. This indicates that increasing the content of the quaternary ammonium ions in the ionomers from 0.2 (in I1) to 0.7 mol% (in I3) leads to the enhanced ionomer adsorption due to the increased binding sites for ionic complexation with CNCs. However, this effect levels off with the further increase in the ionic content in the ionomers from I3 to I6.

In addition, the ionomer modification is found to slightly improve the thermal stability of CNCs. Except mCNC1 and mCNC2, the peak CNC-decomposition temperature of most modified CNCs ($T_{d,max}$, see Table 1) in the first step is generally slightly higher (314−326 ºC) than that of dried unmodified CNCs (311 ºC). With the mCNC3 set of modified samples (mCNC3-1 to mCNC3-4), one can find the increasing trend of $T_{d,max}$ (from 314 to 323 ºC) with increase of the ionomer content from mCNC3-1 to mCNC3-4. These results indicate that the adsorbed ionomers on the surface of modified CNCs can serve as a protecting coating layer enhancing the thermal stability of the CNCs.

Figure 3 shows the XRD pattern of mCNC3-4 as a representative modified CNC sample, along with those of the corresponding ionomer, I3, and dried unmodified CNCs for comparison. Unmodified CNCs show diffraction peaks at 2θ values of 14.7, 17.0, 22.4, and 35.1º, attributed to the (101), $(10\bar{1})$, (002), and (040), respectively, of cellulose I crystal structures.[54] I3 shows a broad diffraction peak centered at 18.3º within the 2θ range, which is the typical amorphous polymer peak found with this range of polyethylene-based ionomers.[49] The diffraction pattern of mCNC3-4 is superimposed by the peaks of both the original CNCs and the ionomer. The characteristic cellulose I diffraction peaks are well retained, confirming as expected that the CNC structures remain intact during this physical surface modification process.

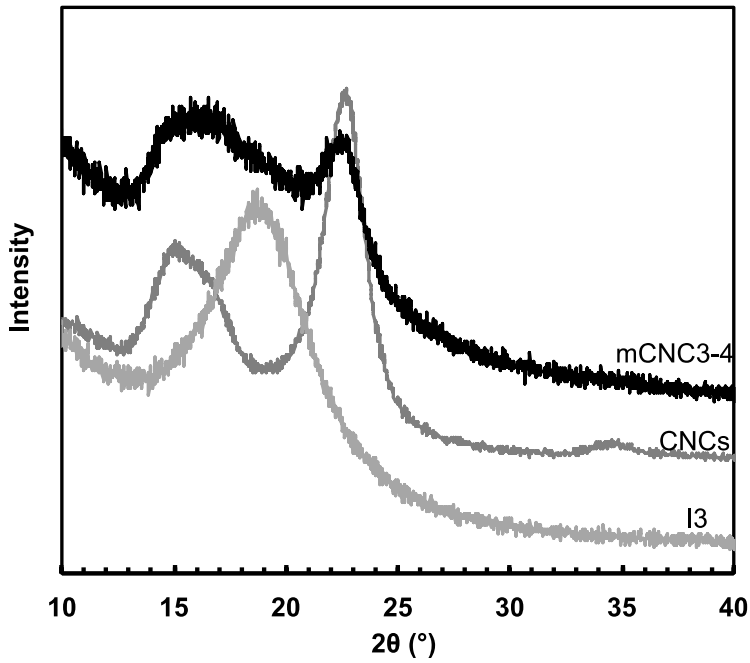

Figure 3. XRD diffraction patterns of mCNC3-4, ionomer I3, and dried unmodified CNCs.

Dilute Dispersions of Modified CNCs in Organic Solvents

Except for mCNC1 and mCNC3-1 due to insufficient ionomer coating, the dried modified CNC powders were found to be dispersible, upon sonication, in nonpolar or low-polarity organic solvents such as toluene, chloroform, and THF at dilute concentrations (around 10 mg mL^{-1}). The dispersions were found stable after ultrasonication for days while freeze-dried unmodified CNCs precipitated out nearly immediately following ultrasonication. However, they were not dispersible in water or high-polarity organic solvents (such as methanol, acetone, etc.) where the hyperbranched polyethylene ionomers themselves cannot disperse/dissolve, confirming the hydrophobic nature of the modified CNCs. Clearly, the dispersibility in these organic solvents can be attributed to the adsorbed ionomers. On the contrary, the large aggregates obtained in the control experiment by dropping the CNC into pure THF without containing ionomers could not disperse THF at all due to the absence of ionomer coating.

DLS measurements were carried out on the dilute dispersions of various modified CNCs in

THF to determine their Z-average hydrodynamic size (d_p), polydispersity index (PDI) of size distribution, and ζ potential. In particular, the data are listed in Table 1. Relative to those of the original CNCs in water (d_p = 91 nm; PDI = 0.3), all the modified CNCs show much greater d_p values (generally within 255–552 nm) and broader distribution (PDI in the range of 0.34–0.56). The higher particle sizes suggest the presence of CNC aggregates as a result of the "cross-linking" effect of the multidentate ionomers. This is further confirmed with the AFM images shown below. The ionomer modification also dramatically changes the ζ potential of the particles. Relative to the negative ζ potential of –27 mV of original CNCs, the set of modified CNC samples (mCNC2, mCNC3-3, mCNC4, mCNC5, and mCNC6) obtained at the same $(m_{ionomer}/m_{CNC})_0$ ratio with different ionomers shows increasing ζ potential values of –15, 17, 20, 22, 30 mV, respectively, with the gradual increase of ionic content in the ionomers. These ζ potential data confirm solidly the expected ionic binding of the cationic ionomers onto the negative charged CNCs, which effectively changes the surface charge of the particles. Particularly, those modified with I3–I6 have reversed charge due to the presence of excess quaternary ammonium cations.

Morphology of Modified CNCs by AFM

AFM imaging of the morphology of modified CNCs was undertaken on samples prepared from their dilute dispersions in THF. Figure 4 shows typical AFM height images of original unmodified CNCs and representative modified CNCs (mCNC2, mCNC3-3, mCNC4, and mCNC6). Their corresponding AFM phase images are shown in Figure S2. Original CNCs (Figure 4a) show a rod-like shape with the average length and width of 119 ± 21 and 5 ± 1 nm, respectively. As opposed to the needle-like shape often observed under transmission electron microscopy, such a rod-like shape is typical of unmodified CNCs under AFM imaging due to the tip-broadening effect.[55] As such, the reported shape width data were all obtained from the AFM height profiles.[55] The ionomer modification dramatically changes the particle morphology by inducing the self-assembled aggregations of individual CNC rods and the rod aggregates (see Scheme 1) due to the "cross-linking" or "bridging" effect of the ionomers. The multidentate nature of the ionomers enables the binding of the different

quaternary ammonium cations present in the same ionomer chain onto different CNC particles, causing the assembly. Meanwhile, the ionic aggregation ubiquitous in ionomers can also make a contribution through the ionic interactions of quaternary ammonium ions present in ionomer chains adsorbed on different CNC particles.

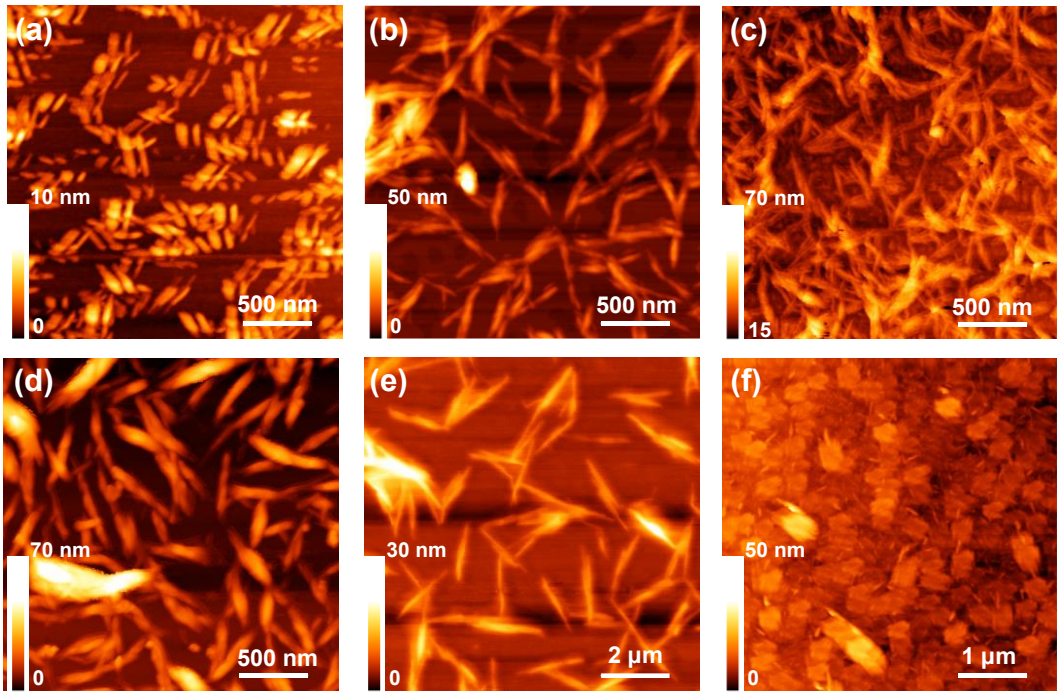

Figure 4. AFM height images of original unmodified CNCs (a), mCNC2 (b); mCNC3-3 (c), mCNC4 (d), mCNC6 (e, f).

In mCNC2, mCNC3-3, and mCNC4, shapes appearing as bundles of CNCs formed through random side-to-side aggregation are extensively present (see Figure 4b-d). In these samples, the average shape length is 170 ± 33, 161 ± 28, and 403 ± 121 nm, respectively; the average width is 9 ± 2, 12 ± 4, and 19 ± 8 nm, respectively. Given the significantly greater shape length and width, the side-to-side aggregation is much more pronounced in mCNC4 than in mCNC2 and mCNC3-3, which is reasoned to result from the higher quaternary ammonium content in the enabling ionomer I4. More interestingly, two unique types of shapes with significantly larger dimensions are observed in mCNC6. Figure 4e shows a high-aspect-ratio, needle-like shape extensively present in mCNC6, which has a large average length of 1.5 ± 0.4 µm and an average width of 8 ± 2 nm, respectively. Its extremely long length indicates the extensive presence of longitudinal aggregation of CNC rods. Similar shapes resulting from

longitudinal aggregation were previously reported on self-assembled duplexed DNA-grafted CNCs.[56] Figure 4f shows another sheet-like shape also extensively present in mCNC6, which is featured with a dimension of (320 ± 35) nm × (235 ± 38) nm, with a thickness of 10 ± 2 nm. This latter shape has not been previously reported for any modified CNCs. Herein, it was only observed in mCNC6 while not in the other modified CNCs. We expect its formation should involve highly ordered side-to-side assembly of the CNC rods. The formation of the two curious types of shapes in mCNC6 is puzzling and suggests future investigation. Given their sole presence in mCNC6, the ionic content of the enabling ionomers clearly plays a significant role in the self-assembly of the modified CNC rods to render the different shapes. On the contrary, the control sample obtained by dropping the neat CNC into pure THF without containing ionomers shows large irregular random aggregates (see Figure S3). A surfactant CTAB-modified CNC sample (CTAB-CNC) was also prepared as another control sample. It also shows dispersibility in THF. Like the ionomer-modified CNCs, its AFM images (Figure S3) also show the presence of aggregates.

A representative AFM image taken on mCNC4 (Figure 5a) also provides some visual evidence confirming the presence of the ionomer coating around the shapes. In the image, every shape appears to be surrounded with a coating layer at the edge, which shows different phase compared to the surrounded area. Figure 5b shows the height profiles for two shapes denoted in Figure 5a, which show the presence of the settled coating layer at a height of around 2.1–3.4 nm.

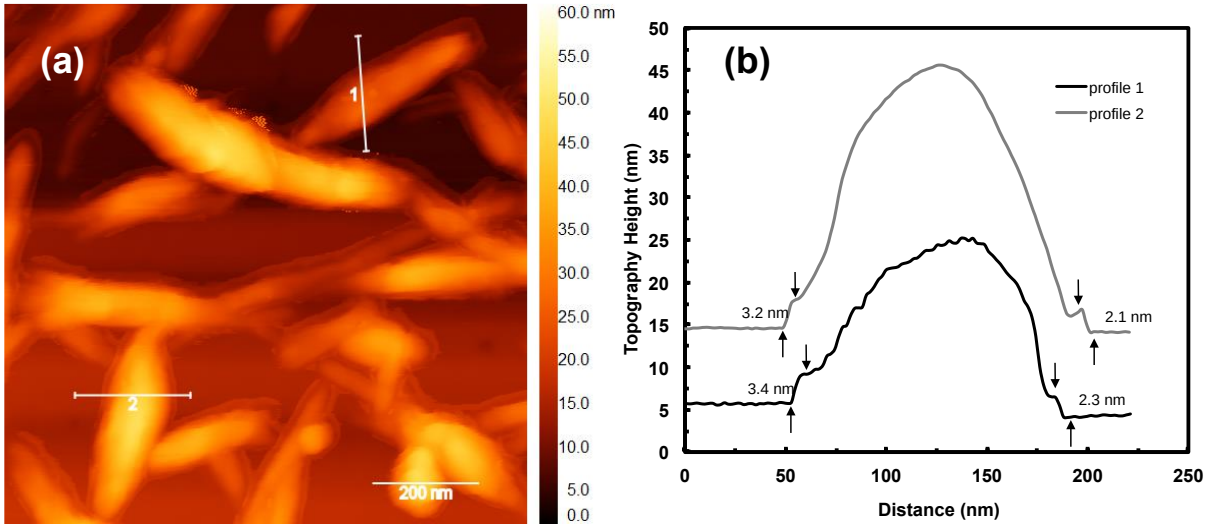

Figure 5. (a) AFM height image of mCNC4 at a higher magnification; (b) height profiles across two shapes denoted in (a).

Thixotropic Behavior of Dispersions of Modified CNCs in THF

Aqueous dispersions of sulfonated CNCs show interesting rheological behavior due to their unique rod-like shape with a charged surface and the tendency to form ordered liquid crystalline structures.[57,58] With the gradual increase of the CNC concentration, aqueous dispersions of CNCs transition from isotropic (CNC concentration ≤ ca. 3 mg mL^{-1}) to a biphasic suspension (ca. 3–10 mg mL^{-1}) and to a birefringent gel-like material (≥ ca. 11 mg mL^{-1}), which in turn changes their rheological properties.[59-61] The temperature,[60] aspect ratio,[62] surface charge,[63,64] addition of electrolytes[65,66] or polymers[67,68] into the aqueous dispersions of CNCs can also dramatically affect their rheological behavior. In addition, aqueous dispersions of HCl-hydrolyzed CNCs[69] and covalently modified cationic CNCs[70] have been reported to behave as thixotropic fluids. However, all the rheological studies have thus far focused on their aqueous dispersions, while with extremely limited study[44] on the dispersions of organo-dispersible CNCs in organic solvents.

The unique dispersibility of the ionomer-modified CNCs in nonpolar or low-polarity organic solvents enables us to study the rheological properties of their dispersions in THF. With mCNC4, we prepared a range of dispersions at different concentrations (10–75 mg mL^{-1}) in

THF. All the dispersions were left standing for a week after preparation. The dispersion at the lowest concentration of 10 mg mL^{-1} was found to remain as a cloudy, readily flowable, isotropic dispersion without precipitation. On the contrary, all the other dispersions (within 25–75 mg mL^{-1}) turned into white-colored organo-gels, suggesting the formation of a network structure in the dispersions. But all the dispersions/gels did not show birefringence, confirming the absence of ordered liquid crystal structures. In particular, the gels with mCNC4 concentration $\geqslant$ 40 mg mL^{-1} remained stable even when their vials were inverted, but became readily flowable after being shaken (Figure 6a,b), indicating the breakdown of the internal structure under shear. Such a behavior is typical of thixotropic fluids. After left standing overnight, the shaken flowable fluids turned back into the invertible gels again, suggesting the rebuilding of the network structure. We found that the round-trip transitions between gel and flowable fluid were reversible for 4 cycles that we examined. The gel formed at the mCNC4 concentration of 25 mg mL^{-1} was, however, not strong enough to support its own weight and flowed down upon the inversion of its vial (Figure 6a).

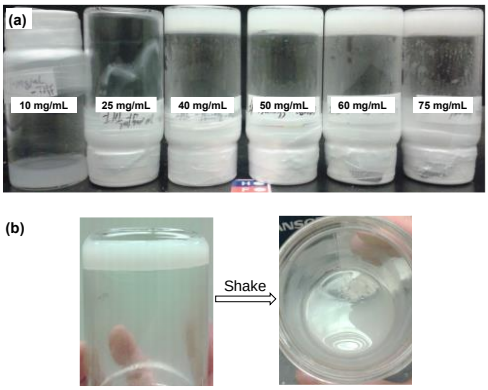

Figure 6. Dispersions and organo-gels of mCNC4 in THF at different concentrations (10–75 mg mL^{-1}) after standing for a week and thixotropic behavior of the gels.

We have also found that the organo-gels only form in THF, while not in other solvents (toluene, chloroform, and chlorobenzene were examined). In these latter solvents, the dispersions, despite at high concentrations (75 mg mL^{-1}), remained as isotropic flowable fluids even after long standing. This indicates the critical role of THF in facilitating the formation of the gel network structure in these dispersions. Clearly, the solvent-particle

interactions contribute significantly to the gel formation. However, the precise mechanism for the formation of organo-gels in THF is not known at the moment and will require further investigation.

Rheological characterization of the dispersions with mCNC4 concentration within 40–75 mg mL^{-1} was undertaken by both small amplitude dynamic oscillation and steady shear measurements at 10 ºC. Figure 7a–d shows the data obtained from the small amplitude dynamic oscillation measurements. At a high strain of 100%, the dispersions behave primarily as viscous fluids with loss modulus (G'') greater than storage modulus (G') and both moduli show frequency dependences (Figure 7a). At a low strain of 0.01%, the dispersions are primarily elastic with G' much greater than G''; G' shows only very weak dependences on frequency, confirming their behavior approaching to ideal stiff gels (Figure 7b). For each dispersion, the complex viscosity (η*) is more than one order of magnitude greater at the strain of 0.01% than at 100% (Figure 7c). The phase angle (δ) values at the strain of 0.01% stay nearly constant around 10 º across the frequency range for all these gels while the values are much greater at the strain of 100% along with the frequency dependences (Figure 7d). With the increase of the concentration of mCNC4 in the dispersions, the moduli and η* values all increase. These oscillation results confirm the transition of the dispersions from elastic gel to viscous fluid following the breakdown of the gel network structure with the increase of strain.

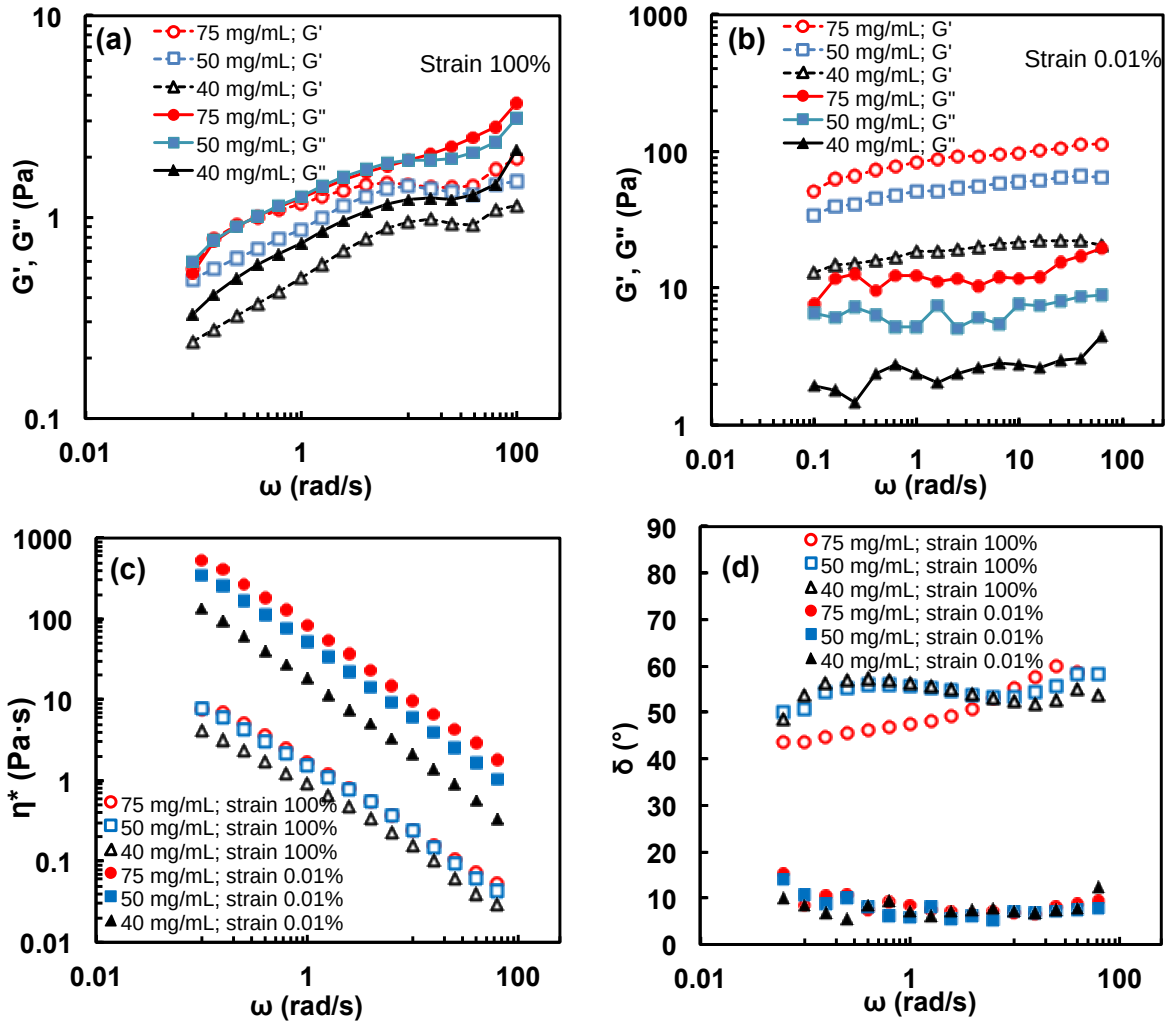

Figure 7. Rheological data from small amplitude dynamic oscillation measurements of organo-gels of mCNC4 in THF at different concentrations (40–75 mg mL^{-1}) at 10 ºC: (a) dynamic moduli (G' and G") vs. frequency (ω) at the strain of 100%; (b) G' and G" vs. ω at the strain of 0.01%; (c) η* vs. ω at both strains of 100% and 0.01%; (d) phase angle (δ) vs. ω at both strains.

Figure 8 plots the viscosity vs. shear rate curves for the dispersions obtained in the steady shear measurements with up and down shear rate sweeps. The three dispersions show similar hysteresis loops characteristic of thixotropic fluids. With the increase of the concentration of mCNC4, the area of the hysteresis loop shows a trend of increase, indicating that the extent of thixotropy increases with the concentration.

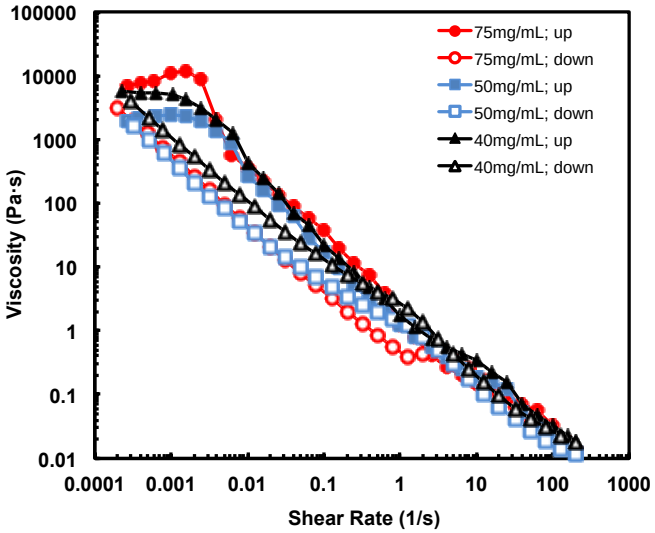

Figure 8. Viscosity vs. shear rate curves of thixotropic organo-gels of mCNC4 in THF at different concentrations (40–75 mg mL^{-1}) obtained through steady shear measurements at 10 ^{o}C.

Dispersions were also prepared with other modified CNCs [mCNC1, mCNC2, mCNC3-3, and mCNC6 prepared at the same $(m_{ionomer}/m_{CNC})_0$ ratio of 2] in THF at the same concentration of 75 mg mL^{-1}. The dispersions of mCNC1 and mCNC2 remained as flowable fluids with no gel formation despite long standing while the others (prepared with mCNC3-3 and mCNC6) turned into thixotropic gels. This distinct difference suggests that the ionomers having varying ionic content employed for their surface modification plays the decisive role in the formation of gel network. Only dispersions of modified CNCs (mCNC3-3, mCNC4, and mCNC6) prepared with ionomers of ionic content ≥ 0.7 mol% have the feature of gel formation. We reason that the higher surface charge and higher shape aspect ratio following the modification of ionomers of high ionic content as shown above are the primary underlying causes of gel formation in these dispersions. It has been shown in earlier studies[62-64] that the surface charge and aspect ratio of sulfated CNCs can significantly affect gel formation.

Figure S4 compares the rheological data of the thixotropic dispersions of mCNC3-3, mCNC4, and mCNC6 obtained from dynamic oscillation measurements at 10 ^{o}C. Like that of mCNC4

shown above, both dispersions of mCNC3-3 and mCNC6 behave as stiff gel at the low strain of 0.01% and turn into flowable fluids at the high strain of 100%. From Figure S4(b), G' of the organo-gels increases in the order of mCNC3-3 < mCNC4 < mCNC6, indicating the stronger inter-particle interactions with the increase of ionic content of the adsorbed ionomer in the modified CNCs. Figure S5 compares the viscosity-shear rate curves obtained from the steady shear measurements on the dispersions of mCNC3-3, mCNC4, and mCNC6. The thixotropic hysteresis loops become bigger by following the same order of mCNC3-3 < mCNC4 < mCNC6. These differences likely result from the increasing surface charge and shape aspect ratio in the set of modified CNCs.

EOC Composites with Modified CNCs as Reinforcing Fillers

The range of ionomer-modified CNCs was further investigated for their dispersion quality and reinforcing performance as fillers in a commercial EOC elastomer as the polymer matrix. Several grades of polyolefins (polyethylenes and polypropylenes) have been previously employed as the polymer matrices for the construction of CNC-filled composites,[32,71-77] but not ethylene-based elastomers. The EOC is chosen here because it should have good compatibility with the highly branched polyethylene skeleton in the ionomers given their structural similarity with high branching density (estimated at ca. 56 branches per 1000 carbons for EOC).[78] Composites were prepared with selected modified CNCs, including mCNC2, mCNC3-3, mCNC4, and mCNC5, at the targeted dry CNC loading of 10 wt% by the solution compounding method. In addition, composites were also prepared with dried unmodified CNCs and surfactant modified CNCs (CTAB-CNC), respectively, as fillers at the same dry CNC loading of 10 wt% for comparison. All resulting composites are named as filler/EOC (see Table 2).

TGA characterization of the composites was conducted. Figure S6 shows their TGA curves and the TGA results are summarized in Table 2. All the composites show a two-step weight loss. For those compounded with ionomer-modified CNCs and unmodified CNCs, the

first-step weight loss occurs between 250 and 320 ºC, which is attributed to the decomposition of CNCs. For that compounded with CTAB-CNC, the first-step weight loss starts much earlier at ca. 200 ºC and is much broader (200–330 ºC), which is attributed to the decomposition/volatilization of both CNCs and the adsorbed CTAB. $T_{d,max}$ of the first step is appreciably higher in the composites compounded with ionomer-modified CNCs (286–308 ºC) than with unmodified CNCs (282 ºC) and CTAB-CNC (284 ºC), confirming again the relatively higher thermal stability of the ionomer-modified CNCs. Attributed primarily to the decomposition of EOC, the second-step weight loss occurs within 350–500 ºC for all the composites. In good agreement with the targeted value of 10 wt%, the mass content of dry CNCs in all composites was quantified, from the first-step TGA weight loss, to be about 10–11 wt%.

DSC characterization was carried out to investigate the effects of the various fillers on the crystallization of the polymer matrix. Figure S7 shows the DSC crystallization exotherms of the various composites, along with that of neat EOC. The DSC results are also summarized in Table 2. Neat EOC shows a low onset crystallization temperature ($T_{c,onset}$) of 42 ºC and a small crystallization heat (ΔH_c) of 57 J/g due to its nature as a branched ethylene copolymer elastomer. The use of unmodified CNCs and CTAB-CNC as fillers leads to the decrease of $T_{c,onset}$ to 41 ºC. In contrast, the composites with the ionomer-modified CNCs as fillers all show appreciably increased $T_{c,onset}$ (43–45 ºC). Meanwhile, it also appears that the composites with ionomer-modified CNCs have slightly lowered ΔH_c (45–49 J/g) relative to those with unmodified CNCs and CTAB-CNC (49–50 J/g). These DSC results suggest that the ionomer-modified CNCs are relatively better dispersed in the EOC matrix than unmodified CNCs and CTAB-CNC and can serve as nucleation agents facilitating the heterogeneous crystallization process.[79] It is known that the better dispersion of fillers helps increase the matrix-filler contact surface area and their interactions, rendering increased $T_{c,onset}$ and reduced ΔH_c.[79]

Table 2. Thermal and mechanical properties of EOC and its composites

Sample	TGA results			DSC results[d]			Tensile properties[e]		
	$T_{d,max}$[a] (ºC)	ΔW_1[b] (%)	Dry CNC content[c] (wt%)	$T_{c,onset}$ (ºC)	ΔH_c (J/g)	T_c (ºC)	σ_{max} (MPa)	ε_{max} (%)	Modulus[e] (MPa)
Neat EOC	N/A	0	0	42	57	46	2.9	1575	4.9
CNC/EOC	282	7	11	41	49	47	2.7	759	10
CTAB-CNC/EOC	284	6	10	41	50	48	2.7	832	9.5
mCNC2/EOC	286	6	10	45	50	52	2.3	1187	7.9
mCNC3-3/EOC	295	6	10	44	48	53	2.5	1099	8.5
mCNC4/EOC	308	7	11	43	49	53	2.5	1037	9.5
mCNC5/EOC	300	7	11	43	45	53	2.6	1071	9.7

[a] Peak decomposition temperature in the first-stage, weight loss within 200–330 ºC. [b] Percentage weight loss in the first-stage within 200–330 ºC. [c] Weight percentage of dry unmodified CNCs in the composites calculated by $\Delta W_1/0.63$. [d] Crystallization onset temperature ($T_{c,onset}$), crystallization temperature (T_c), and crystallization heat (ΔH_c) measured during the cooling step at rate of 10 ºC/min. [e] Maximum tensile strength (σ_{max}), elongation at break (ε_{max}), and Young's modulus determined during tensile tests at 500 mm min^{-1}.

The composites, along with neat EOC, were characterized by small amplitude dynamic oscillation at 190 ºC to study the effects of various fillers on linear melt viscoelastic properties of the samples. Figure 9a,b compare their G' and δ curves, respectively. Neat EOC displays the typical viscous liquid-like behavior with $G' \propto \omega^{1.63}$ ($G'' = \omega^{0.98}$; G" >> G') and $\delta \approx 90^{o}$ in the terminal flow range. The addition of dried unmodified CNCs in CNC/EOC at 10 wt% dramatically enhances G' by more than three orders of magnitude within the low-frequency range, along with a much lowered order (0.38) of dependence on ω. This indicates its solid-like behavior.[75,80] Meanwhile, its δ values are below 45º in the low frequency range, suggesting the presence of the percolated filler network within the composite.[75,80] As such, the dry CNC content of 10 wt% should be above the percolation threshold.

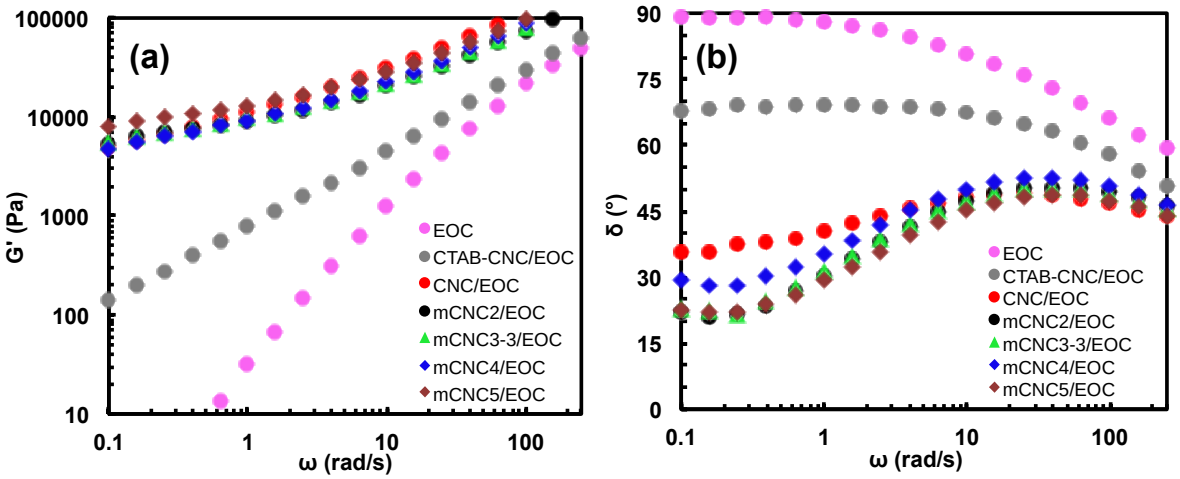

Figure 9. Results from dynamic oscillation measurements of various composites and neat EOC at 190 ºC: G' (a) and δ (b) as functions of frequency.

The effects of CTAB-CNC on the rheological properties, however, are not so dramatic as the unmodified CNCs. CTAB-CNC/EOC still behaves primarily like a viscous liquid though with some level of enhancement in G' relative to neat EOC and the δ value shows a plateau at about 70º in the low frequency range. These results suggest the absence of the percolated filler network in CTAB-CNC/EOC even though the same dry CNC content of 10 wt% was used. This behavior is reasoned to result possibly from the desorption of CTAB or

decomposition of the CTAB-CNC or both in the composite at the high measurement temperature. We found that the sample discs of CTAB-CNC/EOC, prepared by compression molding at 135 ºC for rheology measurements, were yellow-colored as opposed to the white color found with all the other composites. This indicates the presence of decomposition even at 135 ºC when pressed at 2 MPa. The desorbed CTAB or the decomposed low-molecular-weight products or both are reasoned to act as lubricants during the oscillation measurements, rendering viscous liquid-like flow behavior.

The ionomer-modified CNCs instead show even more dramatic effects on the rheological properties than unmodified CNCs. Significant enhancements in G' are noticed with the appearance of a plateau in the low frequency range for each one of them. The enhancements are even more significant in some of the composites than in CNC/EOC shown above. Meanwhile, the δ values of all the composites with modified CNCs are lower than those of CNC/EOC in the low frequency range. Such a flow behavior is commonly observed in percolated composites with increasing filler loading.[75,80] It indicates that not only the percolated filler network is present in all the composites filled with modified CNCs, but also the solid-like behavior is even more pronounced in them with stronger filler-filler and filler-matrix interactions than in CNC/EOC. Given their nearly identical dry CNC content, this rheological behavior is reasoned to result from the better dispersion of the modified CNCs in the EOC matrix. Clearly, the ionomer modification makes the fillers more compatible with the EOC matrix, thus minimizing filler aggregation and increasing filler-matrix interface. In line with the DSC results, the rheological results also confirm the significant improvement caused by ionomer modification upon the dispersibility of the modified CNCs in EOC relative to the unmodified CNCs. Along with the TGA results discussed above, a comparison of their rheological results further verifies the higher thermal stability of ionomer-modified CNCs relative to CTAB-CNC.

The tensile mechanical properties of the various composites were characterized. The results are summarized in Table 2. Figure 10 compares the Young's modulus and elongation at break data of the various composites and neat EOC. It is known that the inclusion of fillers in a

polymer matrix has a reinforcing and stiffening effect, which is usually counteracted by a significant loss in ductility.[78,80] While increases in the moduli of polymer matrices are generally expected upon addition of reinforcing fillers, this reinforcement effect in polymer composites is typically accompanied by a significant reduction in elongation at break because of the presence of large aggregates that create weak spots.[78] These effects have also been observed with various CNC-filled polyolefin composites in earlier studies.[32,71,73,74,76,77] Herein, upon the addition of the various CNC fillers, the modulus is nearly doubled (from 4.8 MPa to 7.9–9.8 MPa) in all the composites, confirming the significant reinforcing effects of all the CNC-based fillers on the EOC. However, different extent of reductions in the elongation at break is found. The reduction is most severe in CNC/EOC and CTAB-CNC/EOC, with their values (759 and 832%, respectively) reduced nearly by half relative to that of neat EOC (1575%). Composites prepared with the ionomer-modified CNCs instead have maintained elongation at break (within the range of 1037–1186%). Relative to CNC/EOC and CTAB-CNC/EOC, their higher elongation at break also confirms the improved dispersion of the modified CNCs in the matrix, as well as the improved interfacial adhesion between the modified CNCs and the matrix following ionomer modification.

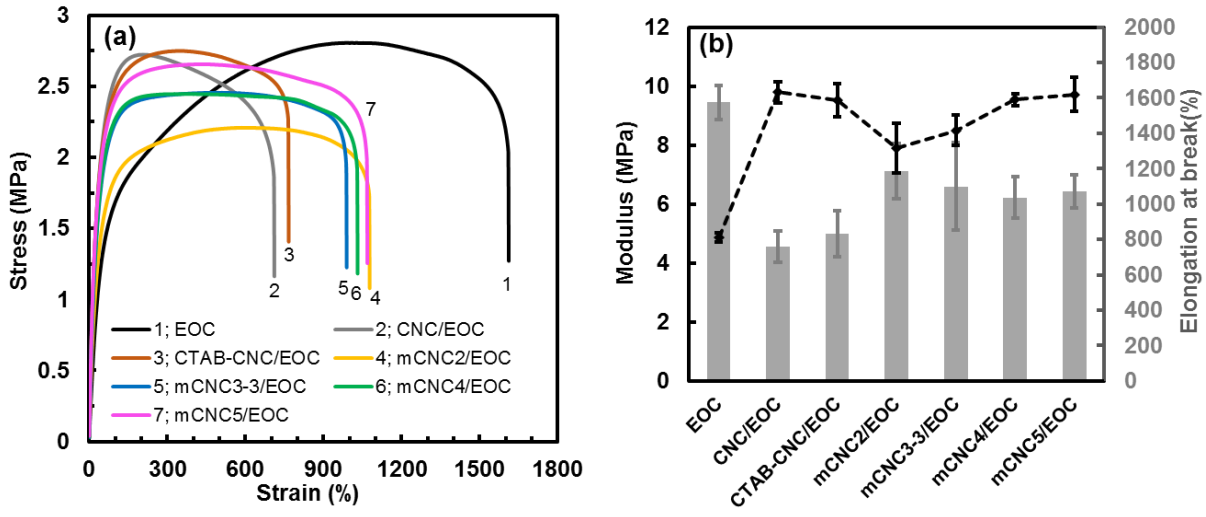

Figure 10. (a) Representative tensile strength vs. strain curves of neat EOC and various composites; (b) Comparison of secant modulus and elongation at break of neat EOC and various composites.

These tensile data thus confirm the advantages of the ionomer modification in improving the

reinforcing performance of CNCs relative to unmodified CNCs and CTAB-modified CNCs. While there is no clear trend of differences observed among the composites compounded with the various ionomer-modified CNCs, mCNC5/EOC shows the optimally balanced tensile properties among the set, with the highest modulus of 9.7 MPa and an elongation at break of 1071%. Though demonstrated herein with the ductile EOC elastomer as the matrix, our findings here may be of significance when other polyolefin matrices are used, which may suffer significant loss in ductility in the presence of CNC-based fillers.

■ Conclusions

A range of quaternary ammonium-containing hyperbranched polyethylene ionomers (I1–I6) with different ionic content (0.2–2.3 mol%) has been synthesized and employed herein for the surface modification of CNCs. The simple addition and mixing of aqueous dispersion of CNCs with a THF solution of the ionomer renders conveniently the modified CNCs, primarily through the multidentate ionic assembly of the positively charged ammonium ions of the ionomers with the negatively charged CNCs. A range of modified CNCs has been prepared with the use of different ionomers. The presence of the adsorbed ionomers in the modified CNCs has been confirmed by FTIR, XRD, and TGA results. Quantification of the content of adsorbed ionomer in the modified CNCs by TGA indicates its increase with the increase of $(m_{ionomer}/m_{CNC})_0$ ratio or the ionic content of the ionomer. AFM imaging of the modified CNCs indicate their significantly enlarged shape size relative to unmodified CNCs, due to the occurrence of side-to-side and/or longitudinal assembly of individual CNCs upon ionomer modification.

Thanks to the hydrophobic hyperbranched polyethylene skeleton, ionomer-modified CNCs are dispersible in nonpolar or low-polarity solvents and hydrophobic EOC matrix. Most modified CNCs (except mCNC1 and mCNC3-1) are dispersible in solvents including THF, toluene, and chloroform. The dispersions of mCNC3-3, mCNC4, and mCNC6 in THF with concentration $\geq$ 40 mg mL^{-1} has been found to behave as thixotropic organo-gels, which act

as stiff gels at low strain (or shear rate) and as viscous fluids at high strain (or shear rate).

In the EOC matrix, the ionomer-modified CNCs show better dispersion as fillers than unmodified CNCs on the basis of the collective results from the thermal, rheological, and tensile mechanical characterizations. Their better dispersion renders stronger filler-filler and matrix-filler interactions. In consequence, the EOC composites filled with the ionomer-modified CNCs are significantly reinforced with nearly doubled modulus relative to neat EOC while with much better maintained elongation at break relative those filled unmodified CNCs or CTAB-CNC.

Though demonstrated specifically with hyperbranched polyethylene-based ionomers herein, this efficient modification strategy should be general and applicable to other quaternary ammonium-containing ionomers. With the availability of various polymerization techniques for such ionomers, a rich variety of ionomer-modified CNCs can be rendered to suit various specific applications.

■ Associated Content

Supporting Information

Summary of synthesis and structural characterization of the ionomers (Table S1); ^{1}H NMR spectra of the ionomers (Figure S1); AFM phase images of unmodified CNCs and modified CNCs (Figure S2); AFM images of control samples (Figure S3); small amplitude dynamic oscillation data of organo-gels of mCNC3-3, mCNC4, and mCNC6 in THF (Figure S4); viscosity-shear rate curves of organo-gels of mCNC3-3, mCNC4, and mCNC6 in THF (Figure S5); TGA curves of the EOC composites (Figure S6); DSC crystallization curves of various EOC composites (Figure S7).

■ Acknowledgement

We thank the Natural Science and Engineering Research Council (NSERC) of Canada for funding this research through an Engage Grant (EGP 47068-14) and a Discovery Grant

(RGPIN-2015-03815). We also thank Dr. Wadood Hamad at FPInnovations (Vancouver, Canada) for helpful discussions and Prof. Jeffrey Shepherd at Laurentian University for the use of AFM in his laboratory.

■ References

(1) De Souza Lima, M. M.; Borsali, R. Rodlike cellulose microcrystals: structure, properties, and applications. *Macromol. Rapid Commun.* **2004**, *25*, 771–787.

(2) Habibi, Y.; Lucian, L. A.; Rojas, O. J. Cellulose nanocrystals: chemistry, self-assembly, and applications. *Chem. Rev.* **2010**, *110*, 3479–3500.

(3) Moon, R. J.; Martini, A.; Nairn, J.; Simonsen, J.; Youngblood, J. Cellulose nanomaterials review: structure, properties and nanocomposites. *Chem. Soc. Rev.* **2011**, *40*, 3941–3994.

(4) Klemm, D.; Kramer, F.; Moritz, S.; Lindström, T.; Ankerfors, M.; Gray, D.; Dorris, A. Nanocelluloses: a new family of nature-based materials. *Angew. Chem. Int. Ed.* **2011**, *50*, 5438–5466.

(5) Lin, N.; Huang, J.; Dufresne, A. Preparation, properties and applications of polysaccharide nanocrystals in advanced functional nanomaterials: a review. *Nanoscale* **2012**, *4*, 3274–3294.

(6) Kelly, J. A.; Giese, M.; Shopsowitz, K. E.; Hamad, W. Y.; MacLachlan, M. J. The development of chiral nematic mesoporous materials. *Acc. Chem. Res.* **2014**, *47*, 1088–1096.

(7) Šturcová, A.; Davies, G. R.; Eichhorn, S. J. Elastic modulus and stress-transfer properties of tunicate cellulose whiskers. *Biomacromolecules* **2005**, *6*, 1055–1061.

(8) Favier, V.; Canova, G. R.; Cavaillé, J. Y.; Chanzy, H.; Dufresne, A.; Gauthier, C. Nanocomposite materials from latex and cellulose whiskers. *Polym. Adv. Technol.* **1995**, *6*, 351–355.

(9) Samir, M. A. S. A.; Alloin, F.; Dufresne, A. Review of recent research into cellulosic whiskers, their properties and their application in nanocomposite field.

Biomacromolecules **2005**, *6*, 612–626.

(10) Mariano, M.; El Kissi, N.; Dufresne, A. Cellulose nanocrystals and related nanocomposites: review of some properties and challenges. *J. Polym. Sci., Part B: Polym. Phys.* **2014**, *52*, 791–806.

(11) Miao, C.; Hamad, W. Y. Cellulose reinforced polymer composites and nanocomposites: a critical review. *Cellulose* **2013**, *20*, 2221–2262.

(12) Shopsowitz, K. E.; Qi, H.; Hamad, W. Y.; MacLachlan, M. J. Free-standing mesoporous silica films with tunable chiral nematic structures. *Nature* **2010**, *468*, 422–425.

(13) Khan, M. K.; Hamad, W. Y.; MacLachlan, M. J. Tunable mesoporous bilayer photonic resins with chiral nematic structures and actuator properties. *Adv. Mater.* **2014**, *26*, 2323–2328.

(14) Giese, M.; Blusch, L. K.; Khan, M. K.; Hamad, W. Y.; MacLachlan, M. J. Responsive mesoporous photonic cellulose films by supramolecular cotemplating. *Angew. Chem. Int. Ed.* **2014**, *53*, 8880–8884.

(15) Giese, M.; Khan, M. K.; Hamad, W. Y.; MacLachlan, M. J. Imprinting of photonic patterns with thermosetting amino-formaldehyde-cellulose composites. *ACS Macro Lett.* **2013**, *2*, 818–821.

(16) Fox, J. D.; Capadona, J. R.; Marasco, P. D.; Rowan, S. J. Bioinspired water-enhanced mechanical gradient nanocomposite films that mimic the architecture and properties of the squid beak. *J. Am. Chem. Soc.* **2013**, *135*, 5167–5174.

(17) Wang, B.; Walther, A. Self-assembled, iridescent, crustacean-mimetic nanocomposites with tailored periodicity and layered cuticular structure. *ACS Nano* **2015**, *9*, 10637–10646.

(18) Roohani, M.; Habibi, Y.; Belgacem, N. M.; Ebrahim, G.; Karimi, A. N.; Dufresne, A. Cellulose whiskers reinforced polyvinyl alcohol copolymers nanocomposites. *Eur. Polym. J.* **2008**, *44*, 2489–2498.

(19) Bardet, R.; Belgacem, N.; Bras, J. Flexibility and color monitoring of cellulose nanocrystal iridescent solid films using anionic or neutral polymers. *ACS Appl. Mater. Interfaces* **2015**, *7*, 4010–4018.

(20) Samir, M. A. S. A; Alloin, F.; Sanchez, J. Y.; Dufresne, A. Cellulose nanocrystals reinforced poly(oxyethylene). *Polymer* **2004**, *45*, 4149–4157.

(21) Pranger, L.; Tannenbaum, R. Biobased nanocomposites prepared by in situ polymerization of furfuryl alcohol with cellulose whiskers or montmorillonite clay. *Macromolecules* **2008**, *41*, 8682–8687.

(22) Querejeta-Fernández, A.; Chauve, G.; Methot, M.; Bouchard, J.; Kumacheva, E. Chiral plasmonic films formed by Gold nanorods and cellulose nanocrystals. *J. Am. Chem. Soc.* **2014**, *136*, 4788–4793.

(23) Thérien-Aubin, H.; Lukach, A.; Pitch, N.; Kumacheva, E. Coassembly of nanorods and nanospheres in suspensions and in stratified films. *Angew. Chem. Int. Ed.* **2015**, *54*, 5618–5622.

(24) Nguyen, T.-D.; Hamad, W. Y.; MacLachlan, M. J. CdS quantum dots encapsulated in chiral nematic mesoporous Silica: new iridescent and luminescent materials. *Adv. Funct. Mater.* **2014**, *24*, 777–783.

(25) Wang, M.; Olszewska, A.; Walther, A.; Malho, J.-M.; Schacher, F. H.; Ruokolainen, J.; Ankerfors, M.; Berglund, L. A.; Österberg, M.; Ikkala, O. Colloidal ionic assembly between anionic native cellulose nanofibrils and cationic block copolymer micelles into biomimetic nanocomposites. *Biomacromolecules* **2011**, *12*, 2074–2081.

(26) Favier, V.; Chanzy, H.; Cavaillé, J. Y. Polymer nanocomposites reinforced by cellulose whiskers. *Macromolecules* **1995**, *28*, 6365–6367.

(27) Hajji, P.; Cavaillé, J. Y.; Favier, V.; Gauthier, C.; Vigier, G. Tensile behavior of nanocomposites from latex and cellulose whiskers. *Polym. Compos.* **1996**, *17*, 612–619.

(28) Annamalai, P. K.; Dagnon, K. L.; Monemian, S.; Foster, E. J.; Rowan, S. J.; Weder, C. Water-responsive mechanically adaptive nanocomposites based on styrene–butadiene rubber and cellulose nanocrystals—processing matters. *ACS Appl. Mater. Interfaces* **2014**, *6*, 967–976.

(29) Dagnon, K. L.; Shanmuganathan, K.; Weder, C.; Rowan, S. J. Water-triggered modulus changes of cellulose nanofiber nanocomposites with hydrophobic polymer matrices. *Macromolecules* **2012**, *45*, 4707–4715.

(30) Habibi, Y. Key advances in the chemical modification of nanocelluloses. *Chem. Soc. Rev.* **2014**, *43*, 1519–1542.

(31) Eyley, S.; Thielemans, W. Surface modification of cellulose nanocrystals. *Nanoscale* **2014**, *6*, 7764–7779.

(32) Ljungberg, N.; Bonini, C.; Bortolussi, F.; Boisson, C.; Heux, L.; Cavaillé, J. Y. New nanocomposite materials reinforced with cellulose whiskers in atactic polypropylene: effect of surface and dispersion characteristics. *Biomacromolecules* **2005**, *6*, 2732–2739.

(33) Lin, N.; Dufresne, A. Physical and/or chemical compatibilization of extruded cellulose nanocrystal reinforced polystyrene nanocomposites. *Macromolecules* **2013**, *46*, 5570–5583.

(34) Habibi, Y.; Dufresne, A. Highly filled bionanocomposites from functionalized polysaccharide nanocrystals. *Biomacromolecules* **2008**, *9*, 1974–1980.

(35) Habibi, Y.; Goffin, A.-L.; Schiltz, N.; Duquesne, E.; Dubois, P.; Dufresne, A. Bionanocomposites based on poly(ε-caprolactone)-grafted cellulose nanocrystals by ring-opening polymerization. *J. Mater. Chem.* **2008**, *18*, 5002–5010.

(36) Morandi, G.; Heath, L.; Thielemans, W. Cellulose nanocrystals grafted with polystyrene chains through surface-initiated atom transfer radical polymerization (SI-ATRP). *Langmuir* **2009**, *25*, 8280–8286.

(37) Wang, H.-D.; Roeder, R. D; Whitney, R. A.; Champagne, P.; Cunningham, M. F. Graft modification of crystalline nanocellulose by Cu(0)-mediated SET living radical polymerization. *J. Polym. Sci., Part A: Polym. Chem.* **2015**, *53*, 2800–2808.

(38) Heux, L.; Chauve, G.; Bonini C. Nonflocculating and chiral-nematic self-ordering of cellulose microcrystals suspensions in nonpolar solvents. *Langmuir* **2000**, *16*, 8210–8212.

(39) Petersson, L. Kvien, I.; Oksman, K. Structure and thermal properties of poly(lactic acid)/cellulose whiskers nanocomposite materials. *Compos. Sci. Technol.* **2007**, *67*, 2535–2544.

(40) Bondeson, D.; Oksman, K. Dispersion and characteristics of surfactant modified cellulose whiskers nanocomposites. *Compos. Interfaces* **2007**, *14*, 617–630.

(41) Kim, J.; Montero, G.; Habibi, Y.; Hinestroza, J. P.; Genzer, J.; Argyropoulos, D. S.; Rojas, O. J. Dispersion of cellulose crystallites by nonionic surfactants in a hydrophobic polymer matrix. *Polym. Eng. Sci.* **2009**, *49*, 2054–2061.

(42) Salajková, M.; Berglund, L. A.; Zhou, Q. Hydrophobic cellulose nanocrystals modified with quaternary ammonium salts. *J. Mater. Chem.* **2012**, 22, 19798–19805.

(43) Padalkar, S.; Capadona, J. R.; Rowan, S. J.; Weder, C.; Won, Y.-H.; Stanciu, L. A.; Moon, R. J. Natural biopolymers: novel templates for the synthesis of nanostructures. *Langmuir* **2010**, *26*, 8497–8502.

(44) Abitbol, T.; Marway, H.; Cranston, E. D. Surface modification of cellulose nanocrystals with cetyltrimethylammonium bromide. *Nord. Pulp Pap. Res. J.* **2014**, *29*, 46–57.

(45) Zhou, Q.; Brumer, H.; Teeri, T. T. Self-organization of cellulose nanocrystals adsorbed with xyloglucan oligosaccharide-poly(ethylene glycol)-polystyrene triblock copolymer. *Macromolecules* **2009**, *42*, 5430–5432.

(46) Cranston, E. D.; Gray, D. G. Morphological and optical characterization of polyelectrolyte multilayers incorporating nanocrystalline cellulose. *Biomacromolecules* **2006**, *7*, 2522–2530.

(47) Aloulou, F.; Boufi, S.; Beneventi, D. Adsorption of organic compounds onto polyelectrolyte immobilized-surfactant aggregates on cellulosic fibers. *J. Colloid Interface Sci.* **2004**, *280*, 350–358.

(48) Mecking, S.; Johnson, L. K.; Wang, L.; Brookhart, M. Mechanistic studies of the palladium-catalyzed copolymerization of ethylene and α-olefins with methyl acrylate. *J. Am. Chem. Soc.* **1998**, *120*, 888−899.

(49) Xiang, P.; Ye, Z. Hyperbranched polyethylene Ionomers containing cationic tetralkylammonium ions synthesized by Pd–diimine-catalyzed direct ethylene copolymerization with ionic liquid comonomers. *Macromolecules* **2015**, *48*, 6096−6107.

(50) Dong, Z.; Ye, Z. Hyperbranched polyethylenes by chain walking polymerization: synthesis, properties, functionalization, and applications. *Polym. Chem.* **2012**, *3*, 286–301.

(51) Ye, Z.; Xu, L.; Dong, Z.; Xiang, P. Designing polyethylenes of complex chain architectures via Pd–diimine-catalyzed ‘‘living’’ ethylene polymerization. *Chem. Commun.* **2013**, *49*, 6235–6255.

(52) Espinosa, S. C.; Kuhnt, T.; Foster, E. J.; Weder, C. Isolation of thermally stable cellulose nanocrystals by phosphoric acid hydrolysis. *Biomacromolecules* **2013**, *14*, 1223−1230.

(53) Roman, M.; Winter, W. T. Effect of sulfate groups from sulfuric acid hydrolysis on the thermal degradation behavior of bacterial cellulose. *Biomacromolecules* **2004**, *5*, 1671−1677.

(54) Xu, X.; Liu, F.; Jiang, L.; Zhu, J. Y.; Haagenson, D.; Wiesenborn, D. P. Cellulose nanocrystals vs. cellulose nanofibrils: a comparative study on their microstructures and effects as polymer reinforcing agents. *ACS Appl. Mater. Interfaces* **2013**, *5*, 2999−3009.

(55) Kvien, I.; Tanem, B. S.; Oksman, K. Characterization of cellulose whiskers and their nanocomposites by atomic force and electron microscopy. *Biomacromolecules* **2005**, *6*, 3160−3165.

(56) Mangalam, A. P.; Simonsen, J.; Benight, A. S. Cellulose/DNA hybrid nanomaterials. *Biomacromolecules* **2009**, *10*, 497−504.

(57) Beck-Candanedo, S.; Roman, M.; Gray, D. G. Effect of reaction conditions on the properties and behavior of wood cellulose nanocrystal suspensions. *Biomacromolecules* **2005**, *6*, 1048−1054.

(58) Revol, J.-F.; Godbout, L.; Dong, X.-M.; Gray, D. G.; Chanzy, H.; Maret, G. Chiral nematic suspensions of cellulose crystallites; phase separation and magnetic field orientation. *Liq. Cryst.* **1994**, *16*, 127−134.

(59) Bercea, M.; Navard, P. Shear Dynamics of aqueous suspensions of cellulose whiskers. *Macromolecules* **2000**, *33*, 6011−6016.

(60) Ureña-Benavides, E. E.; Ao, G.; Davis, V. A.; Kitchens, C. L. Rheology and phase behavior of lyotropic cellulose nanocrystal suspensions. *Macromolecules* **2011**, *44*, 8990−8998.

(61) Shafiei-Sabet, S.; Hamad, W. Y.; Hatzikiriakos, S. G. Rheology of nanocrystalline

cellulose aqueous suspensions. *Langmuir* **2012**, *28*, 17124−17133.

(62) Wu, Q.; Meng, Y.; Wang, S.; Li, Y.; Fu, S.; Ma, L.; Harper, D. Rheological behavior of cellulose nanocrystal suspension: Influence of concentration and aspect ratio. *J. Appl. Polym. Sci.* **2014**, *131*, 40525.

(63) Araki, J.; Wada, M.; Kuga, S.; Okano, T. Influence of surface charge on viscosity behavior of cellulose microcrystal suspension. *J. Wood Sci.* **1999**, *45*, 258−261.

(64) Shafeiei-Sabet, S.; Hamad, W. Y.; Hatzikiriakos, S. G. Influence of degree of sulfation on the rheology of cellulose nanocrystal suspensions. *Rheol. Acta* **2013**, *52*, 741–751.

(65) Dong, X. M.; Kimura, T.; Revol, J.-F.; Gray, D. G. Effects of ionic strength on the isotropic−chiral nematic phase transition of suspensions of cellulose crystallites. *Langmuir* **1996**, *12*, 2076–2082.

(66) Boluk, Y.; Lahiji, R.; Zhao, L.; McDermott, M. T. Suspension viscosities and shape parameter of cellulose nanocrystals (CNC). *Colloids Surf. A: Physicochem. Eng. Asp.* **2011**, *377*, 297–303.

(67) Boluk, Y.; Zhao, L.; Incani, V. Dispersions of nanocrystalline cellulose in aqueous polymer solutions: structure formation of colloidal rods. *Langmuir* **2012**, *28*, 6114–6123.

(68) Hu, Z.; Cranston, E. D.; Ng, R.; Pelton, R. Tuning cellulose nanocrystal gelation with polysaccharides and surfactants. *Langmuir* **2014**, *30*, 2684–2692.

(69) Araki, J.; Wada, M.; Kuga, S.; Okano, T. Flow properties of microcrystalline cellulose suspension prepared by acid treatment of native cellulose. *Colloids Surf. A: Physiochem. Eng. Asp.* **1998**, *142*, 75–82.

(70) Hasani, M.; Cranston, E. D.; Westman, G.; Gray, D. G. Cationic surface functionalization of cellulose nanocrystals. *Soft Matter* **2008**, *4*, 2238–2244.

(71) Ljungberg, N.; Cavaillé, J.-Y.; Heux, L. Nanocomposites of isotactic polypropylene reinforced with rod-like cellulose whiskers. *Polymer* **2006**, *47*, 6285–6292.

(72) Azouz, K. B.; Ramires, E. C.; Van den Fonteyne, W.; El Kissi, N.; Dufresne, A. Simple method for the melt extrusion of a cellulose nanocrystal reinforced hydrophobic polymer. *ACS Macro Lett.* **2012**, *1*, 236–240.

(73) Pereda, M.; El Kissi, N.; Dufresne, A. Extrusion of polysaccharide nanocrystal reinforced polymer nanocomposites through compatibilization with poly(ethylene oxide). *ACS Appl. Mater. Interfaces* **2014**, *6*, 9365–9375.

(74) De Menezes, A. J.; Siqueira, G.; Curvelo, A. A. S.; Dufresne, A. Extrusion and characterization of functionalized cellulose whiskers reinforced polyethylene nanocomposites. *Polymer* **2009**, *50*, 4552–4563.

(75) Khoshkava, V.; Kamal, M. R. Effect of cellulose nanocrystals (CNC) particle morphology on dispersion and rheological and mechanical properties of polypropylene/CNC nanocomposites. *ACS Appl. Mater. Interfaces* **2014**, *6*, 8146–8157.

(76) Sapkota, J.; Jorfi, M.; Weder, C.; Foster, E. J. Reinforcing poly(ethylene) with cellulose nanocrystals. *Macromol. Rapid Commun.* **2014**, *35*, 1747–1753.

(77) Iyer, K. A.; Schueneman, G. T.; Torkelson, J. M. Cellulose nanocrystal/polyolefin biocomposites prepared by solid-state shear pulverization: Superior dispersion leading to synergistic property enhancements. *Polymer* **2015**, *56*, 464–475.

(78) Xiang, P.; Petrie, K.; Kontopoulou, M.; Ye, Z.; Subramanian, R. Tuning structural parameters of polyethylene brushes on silica nanoparticles in surface-initiated ethylene “living” polymerization and effects on silica dispersion in a polyolefin matrix. *Polym. Chem.* **2013**, *4*, 1381–1395.

(79) Gopakumar, T. G.; Lee, J. A.; Kontopoulou, M.; Parent, J. S. Influence of clay exfoliation on the physical properties of montmorillonite/polyethylene composites. *Polymer* **2002**, *43*, 5483−5491.

(80) Bailly, M.; Kontopoulou, M.; El Mabrouk, K. Effect of polymer/filler interactions on the structure and rheological properties of ethylene-octene copolymer/nanosilica composites. *Polymer* **2010**, *51*, 5506−5515.

TOC Graphics for TOC Use Only

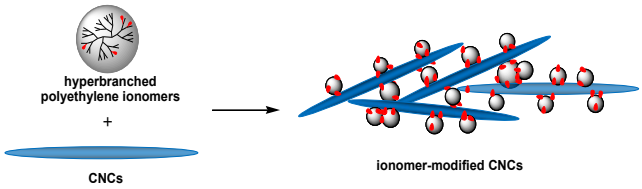

Modification of Cellulose Nanocrystals with Quaternary Ammonium-Containing Hyperbranched Polyethylene Ionomers by Ionic Assembly

Lingqi Huang, Zhibin Ye,* and Richard Berry

Synopsis

A new ionomer functionalization strategy is demonstrated for rendering modified cellulose nanocrystals as a sustainable class of bionanofillers for better reinforced polymer nanocomposites.